PCCP

Accepted Manuscript

ROYAL SOCIETY OF CHEMISTRY

www.rsc.org/pccp

Dynamic and Static Behavior of the H---π and E---π Interactions in EH_2 Adducts of Benzene π-System (E = O, S, Se and Te), Elucidated by QTAIM Dual Functional Analysis

Satoko Hayashi,*[,a] Yuji Sugibayashi[a] and Waro Nakanishi*[,a]

Received (in XXX, XXX) 7th October 2015, Accepted XXX YYY 2015
First published on the web 7th October 2015
DOI: 10.1039/b000000x

Dynamic and static behavior of the interactions in the EH_2 adducts of benzene π-system (E = O, S, Se and Te) is elucidated by applying QTAIM-DFA (QTAIM dual functional analysis). Two types of the H-∗-π and E-∗-π interactions are detected in the adducts, where the asterisk (∗) emphasizes the existence of the bond critical point (BCP) on the interaction in question. Total electron energy densities $H_b(\boldsymbol{r}_c)$ are plotted versus $H_b(\boldsymbol{r}_c) - V_b(\boldsymbol{r}_c)/2$ [$= (\hbar^2/8m)\nabla^2\rho_b(\boldsymbol{r}_c)$] at BCPs in QTAIM-DFA, where $V_b(\boldsymbol{r}_c)$ are the potential energy densities at BCPs. Data from the fully optimized structures are analyzed by the polar (R, θ) coordinate representation. Each plot for an interaction, containing data from the perturbed structures with those of the fully optimized one, shows a specific curve, which provides important information. The plot is expressed by (θ_p, κ_p): θ_p corresponds to the tangent line for the plot and κ_p is the curvature. θ and θ_p are measured from the y-axis and y-direction, respectively. While (R, θ) correspond to the static nature, (θ_p, κ_p) represent the dynamic nature of interactions. While θ classifies the interaction in question, θ_p characterizes it. Both values are less than 90º for all H-∗-π and E-∗-π interactions examined in this work, therefore, they are all classified by the *pure* closed-shell interactions and predicted to have the character of the vdW nature. However, it is suggested that E-∗-π has the nature of the stronger interaction than the case of H-∗-π for the dynamic behavior, in the same species evaluated at the MP2 and M06-2X levels. The nature of the interactions is well analyzed and specified by applying QTAIM-DFA.

Introduction

Hydrogen bonds (HBs) play a very important role in all fields of chemical and biological sciences and they are fundamentally important by their ability of the molecular association due to the stabilization of the system in energy.[1–32] We reported the dynamic and static behavior of HBs of the X–H-∗-π type in benzene π-system, X–H-∗-π(C_6H_6), where X = F, Cl, Br, I, HO, MeO, H_2N, MeHN and Me_2N,[33] after clarification of the behavior in the conventional HBs of the shared proton interaction type.[34] The asterisk (∗) in X–H-∗-π(C_6H_6) emphasizes the existence of the bond critical point (BCP) on the interaction in question. BCP of (ω, σ) = (3, –1)[35] is a point along the bond path (BP) at the interatomic surface, where charge density $\rho(\boldsymbol{r})$ reaches a minimum.[36]

Benzene–water complex has been widely investigated experimentally and theoretically. Suzuki first clarified the structure of the complex through the rotationally resolved spectra supported by the theoretical investigation.[37a] The π-hydrogen bond formation was also observed between liquid water and benzene.[38] The water–benzene binding energy curve was investigated employing various methods.[39] The basis set dependence of solute–solvent interaction energies was computed, which suggested the importance of the corrections of basis set superposition error (BSSE).[40] The structural feature of the complex was also clarified in detail mainly at the DFT levels.[41]

Two structures were optimized for the OH_2 adducts with C_6H_6 as minima at the MP2 level, in our previous investigation.[33] The optimized structures retained the C_s and C_2 symmetries. They were called type Ia_{Bzn} and type II_{Bzn}, respectively, and denoted by HO–H---π(C_6H_6) (C_s: type Ia_{Bzn}) and OH_2---π(C_6H_6) (C_2: type II_{Bzn}), respectively (see Chart 1). However, one imaginary frequency is predicted for OH_2---π(C_6H_6) (C_2: type II_{Bzn}) under our calculation conditions at the MP2 level, although HO–H---π(C_6H_6) (C_s: type Ia_{Bzn}) is predicted to have all positive frequencies. It should be assigned to a transition state (TS) for OH_2---π(C_6H_6) (C_2: type II_{Bzn}) with one imaginary frequency. The results supported the previous observations by Suzuki[37a] and Ben-Amotz.[38]

What happens in OH_2---π(C_6H_6) (C_2: type II_{Bzn})? We considered that the very gradual energy surface around the

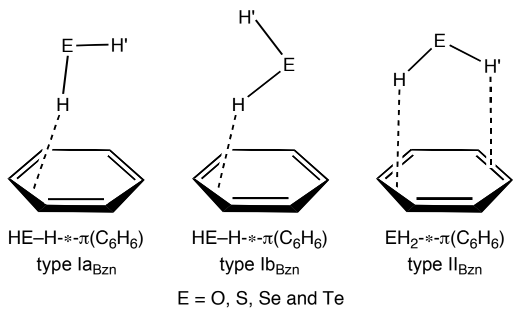

Chart 1 Optimized structures for the EH_2 adducts of benzene π-system (E = O, S, Se and Te).

motion would be responsible for the imaginary frequency under our calculation conditions at the MP2 level. Are the structures of the EH_2 adducts of benzene π-system (E = S, Se and Te) substantially the same as those for E = O? Is the behavior of the interactions in the adducts with E = S, Se and Te similar to that with E = O? To answer these questions, the behavior of the interactions in OH_2-∗-π(C_6H_6) (C_2: type II_{Bzn}) was further investigated. The structural feature was also clarified for the EH_2 adducts with benzene (E = S, Se and Te), together with the behavior of the interactions in the EH_2 adducts of benzene (E = S, Se and Te), as the extension of the interactions in OH_2-∗-π(C_6H_6). Chart 1 illustrates the structures optimized for the EH_2 adducts of benzene π-system (E = O, S, Se and Te).

QTAIM (the quantum theory of atoms-in-molecules) approach, introduced by Bader,[35,42] enables us to analyze the nature of chemical bonds and interactions.[35,42–44] Recently, we proposed QTAIM-DFA (QTAIM dual functional analysis),[45–47] for experimental chemists to analyze their own results, which concerns chemical bonds and interactions by their own image. QTAIM-DFA will provide an excellent possibility to evaluate, understand and classify weak to strong interactions in a unified form.[45–48] QTAIM-DFA is applied to typical chemical bonds and interactions and rough criteria are established, which can distinguish the chemical bonds and interactions in question from others. QTAIM-DFA and the criteria are explained in the Supporting Information, employing Schemes S1 and S2, Figure S1 and eqns (S1)–(S7). The basic concept of the QTAIM approach is also surveyed.

QTAIM-DFA is now applied to elucidate the dynamic and static behavior of the interactions in the EH_2 adducts with benzene π-system (E = O, S, Se and Te). Here, we present the results of the investigations on the nature of the interactions in question. The interactions are classified and characterized by employing the criteria, as a reference.

Methodological details in calculations

Structures were optimized using the Gaussian 09 programs.[49] The 6-311+G(3df) basis set[50] was employed for O, S and Se and the basis set of the (7433211/743111/7411/2 + 1s1p1d1f) type[51] was for Te with the 6-311++G(d,p) basis set for C and H. The basis set system (BSS) is called BSS-F, after the examination of BSSs in the previous paper.[33] The Møller-Plesset second order energy correlation (MP2) level was applied to the calculations.[52] The DFT levels of M06-2X[53] and M06[53] were also applied for the investigations. Optimized structures were confirmed by the frequency analysis, containing those of the components, EH_2 and C_6H_6. Energies of the adducts on the energy surface (E_{ES}) and the lowest two frequencies (ν_1 and ν_2) are given in Table S1 of the Supporting Information, evaluated at the MP2, M06-2X and M06 levels. The structures were also optimized by applying the counterpoise correction method for the adducts at the MP2, M06-2X and M06 levels. The structural parameters by the counterpoise method are shown in Table S2 of the Supporting Information (see, Chart S1 and Scheme S3 for the structural parameters). The counterpoise corrected energies (E_{CP}) and the energies for the basis set superposition errors (E_{BSSE}) are given in Table S3 of the Supporting Information. Table S3 also contains the energies for the formation of the complexes, uncorrected and corrected by E_{BSSE} (denoted by ΔE_{raw} and ΔE_{BSSE}, respectively).

QTAIM functions were calculated using the Gaussian 09 program package[49] with the same method of the optimizations and the data were analyzed with the AIM2000 program.[54] Normal coordinates of internal vibrations (NIV) obtained by the frequency analysis were employed to generate the perturbed structures.[47,48] The method is explained in eqn (1). A k-th perturbed structure in question ($\mathbf{S}_{kw}$) was generated by the addition of the normal coordinates of the k-th internal vibration ($\mathbf{N}_k$) to the standard orientation of a fully optimized structure ($\mathbf{S}_o$) in the matrix representation.[47] The coefficient f_{kw} in eqn (1) controls the difference in the structures between $\mathbf{S}_{kw}$ and $\mathbf{S}_o$: f_{kw} are determined to satisfy eqn (2) for an interaction in question, where r and r_o stand for the distances in question in the perturbed and fully optimized structures, respectively, with a_o of Bohr radius (0.52918 Å). Namely, the perturbed structures with NIV correspond to those with r being elongated or shortened by $0.05a_o$ or $0.1a_o$, relative to r_o, as shown in eqn (2). $\mathbf{N}_k$ of five digits are used to predict $\mathbf{S}_{kw}$. We call this method to generate the perturbed structures NIV. NIV corresponds to the amplification of the selected motion in the zero-point internal vibrations to the extent where r satisfies eqn (2). The selected vibration must contain the motion of the interaction in question most effectively among all zero-point internal vibrations.

$$\mathbf{S}_{kw} = \mathbf{S}_o + f_{kw}\bullet\mathbf{N}_k \quad (1)$$

$$r = r_o + wa_o \quad (2)$$

(w = (0), ±0.05 and ±0.1; a_o = 0.52918 Å)

$$y = a_o + a_1x + a_2x^2 + a_3x^3 \quad (3)$$

(R_c^2: square of correlation coefficient)

In the QTAIM-DFA treatment, $H_b(\boldsymbol{r}_c)$ are plotted versus $H_b(\boldsymbol{r}_c) - V_b(\boldsymbol{r}_c)/2$ for the data of five points for w = 0, ±0.05 and ±0.1 in eqn (2). Each plot is analyzed using a regression curve of the cubic function as shown in eqn (3), where $(x, y) = (H_b(\boldsymbol{r}_c) - V_b(\boldsymbol{r}_c)/2, H_b(\boldsymbol{r}_c))$ ($R_c^2 > 0.99999$ in usual).[45–48,55]

Results and Discussion

Structural Optimizations for the EH_2 Adducts of Benzene π-System (E = O, S, Se and Te)

Structures were optimized for the EH_2 adducts with benzene π-system (E = O, S, Se and Te), employing BSS-F at the MP2 level, together with the DFT levels of M06-2X and M06. Table 1 collects the structural parameters, r_1, r_2, r_3, θ_1, θ_2, θ_2, ϕ_1, ϕ_2 and ϕ_3, which are defined in Scheme 1. The optimized structures are not shown in figures but some of them can be found in Fig. 2, where the molecular graphs are drawn on the optimized structures. Table 1 contains the ΔE_{ES} and ΔE_{ZP} values for the species, evaluated at the MP2, M06-2X and M06 levels. The values are defined by $\Delta E_{ES} = E_{ES}((EH_2)$-∗-π$(C_6H_6)) - (E_{ES}(EH_2) + E_{ES}(C_6H_6))$ on the energy surface and $\Delta E_{ZP} = E_{ZP}((EH_2)$-∗-π$(C_6H_6)) - (E_{ZP}(EH_2) + E_{ZP}(C_6H_6))$, considering the zero-point energy corrections. Table 1 also

Table 1 Structural parameters for the EH_2 adducts with benzene π-system and the energies for the formation of the adducts on the energy surface and those containing the zero-point energy corrections, optimized at the MP2, M06-2X and M06 levels with BSS-F, together with the structural parameters optimized by applying the counterpoise correction method at the MP2 level with BSS-F and the energies for the formation of the adducts[a]

Species (X---Y) (symmetry: type)	r_1 (Å)	r_2 (Å)	r_3 (Å)	θ_1 (°)	θ_2 (°)	θ_3 (°)	ϕ_1 (°)	ϕ_2 (°)	ϕ_3 (°)	ΔE_{ES}[b] (kJ mol^{-1})	ΔE_{ZP}[c] (kJ mol^{-1})
MP2 level											
HO–H---π(C_6H_6) (C_s: type Ia_{Bzn})	2.3824	0.9635	0.9607	81.7	166.5	104.2	-85.1	-149.6	0.0	-17.9	-16.9
HS–H---π(C_6H_6) (C_s: type Ib_{Bzn})	2.4409	1.3385	1.3373	85.9	148.3	92.9	-87.7	-149.9	180.0	-18.2	-18.3
HSe–H---π(C_6H_6) (C_s: type Ib_{Bzn})	2.5340	1.4583	1.4588	83.6	128.4	92.1	-86.3	-149.8	180.0	-19.8	-19.7
HTe–H---π(C_6H_6) (C_s: type Ib_{Bzn})	2.6848	1.6557	1.6595	82.8	111.1	91.3	-85.8	-149.7	180.0	-27.3	-26.3
OH_2---π(C_6H_6) (C_2: type II_{Bzn})[d]	3.3195	0.9623	0.9623	90.0	51.5	103.0	90.0	-30.0	0.0	-16.2	-17.7
SH_2---π(C_6H_6) (C_2: type II_{Bzn})[d]	3.7269	1.3382	1.3382	90.0	45.7	91.4	90.0	-30.0	0.0	-16.7	-18.8
SeH_2---π(C_6H_6) (C_2: type II_{Bzn})[d]	3.8200	1.4584	1.4584	90.0	45.2	90.4	90.0	-30.0	0.0	-17.3	-19.4
TeH_2---π(C_6H_6) (C_2: type II_{Bzn})[d]	3.9656	1.6556	1.6556	90.0	45.2	90.4	90.0	-30.0	0.0	-20.8	-22.6
SH_2---π(C_6H_6) (C_2: type II'_{Bzn})[e,f]	3.7290	1.3382	1.3382	90.0	45.7	91.4	90.0	0.0	0.0	-16.7	-19.0
TeH_2---π(C_6H_6) (C_2: type II'_{Bzn})[e,f]	3.9702	1.6556	1.6556	90.0	45.2	90.3	90.0	0.0	0.0	-20.7	-22.8
M06-2X level											
HO–H---π(C_6H_6) (C_s: type Ia_{Bzn})	2.5586	0.9619	0.9601	78.8	126.0	103.6	-83.4	-149.3	0.0	-17.8	-11.8
	2.9223[g]	0.9601[g]	0.9619[g]	74.4[g]	99.3[g]	103.6[g]	-80.7[g]	-148.7[g]	0.0[g]		
HS–H---π(C_6H_6) (C_s: type Ia_{Bzn})	2.5446	1.3399	1.3368	84.2	145.2	92.0	-86.7	-149.8	0.0	-14.9	-8.5
HSe–H---π(C_6H_6) (C_1: type Ia_{Bzn})	2.5350	1.4676	1.4657	84.9	147.6	91.0	-87.0	-149.8	0.0	-14.5	-8.7
HTe–H---π(C_6H_6) (C_s: type Ia_{Bzn})	2.6304	1.6680	1.6667	84.4	137.8	91.7	-86.8	-149.8	0.0	-14.2	-5.6
HS–H---π(C_6H_6) (C_s: type Ib_{Bzn})[d]	2.5508	1.3389	1.3385	86.4	127.4	92.9	-87.9	-149.9	180.0	-14.7	-11.1
HSe–H---π(C_6H_6) (C_s: type Ib_{Bzn})	2.5551	1.4681	1.4674	85.5	127.8	91.8	-87.4	-149.9	180.0	-15.5	-9.7
HTe–H---π(C_6H_6) (C_s: type Ib_{Bzn})	2.6926	1.6669	1.6687	84.3	116.1	91.9	-86.7	-149.8	180.0	-18.2	-11.4
OH_2---π(C_6H_6) (C_2: type II_{Bzn})	3.2156	0.9611	0.9611	90.0	51.8	103.5	90.0	-27.3	0.0	-17.8	-12.9
SH_2---π(C_6H_6) (C_2: type II'_{Bzn})[f]	3.7047	1.3382	1.3382	90.1	45.8	91.5	-89.9	7.2	0.0	-14.4	-9.5
SeH_2---π(C_6H_6) (C_2: type II_{Bzn})	3.8168	1.4680	1.4680	90.1	45.2	90.5	90.0	-30.0	0.0	-13.7	-8.6
TeH_2---π(C_6H_6) (C_2: type II_{Bzn})	4.0274	1.6670	1.6670	90.1	45.6	91.2	90.0	-19.7	0.0	-12.6	-4.4
M06 level											
HO–H---π(C_6H_6) (C_s: type Ia_{Bzn})	2.7332	0.9613	0.9597	74.9	123.4	103.8	-81.0	-148.8	0.0	-13.7	-8.3
HS–H---π(C_6H_6) (C_s: type Ia_{Bzn})	2.6596	1.3467	1.3431	77.3	145.2	91.8	-82.5	-149.2	0.0	-12.5	-7.3
HSe–H---π(C_6H_6) (C_s: type Ia_{Bzn})	2.6457	1.4733	1.4706	79.8	142.9	91.3	-84.0	-149.4	0.0	-12.4	-8.3
HTe–H---π(C_6H_6) (C_s: type Ia_{Bzn})	2.7705	1.6743	1.6721	79.0	131.9	91.0	-83.6	-149.4	0.0	-11.5	-8.7
HS–H---π(C_6H_6) (C_s: type Ib_{Bzn})	2.6956	1.3455	1.3435	85.0	124.4	92.5	-87.1	-149.8	180.0	-11.3	-6.2
HSe–H---π(C_6H_6) (C_s: type Ib_{Bzn})	2.7034	1.4716	1.4714	84.8	121.6	92.0	-87.0	-149.8	180.0	-13.1	-8.4
HTe–H---π(C_6H_6) (C_s: type Ib_{Bzn})	2.8875	1.6729	1.6755	84.8	110.6	91.2	-87.0	-149.8	180.0	-15.0	-10.6
OH_2---π(C_6H_6) (C_2: type II_{Bzn})	3.3607	0.9603	0.9603	90.0	51.9	103.8	90.0	-28.2	0.0	-13.7	-8.4
SH_2---π(C_6H_6) (C_1: type II_{Bzn})	3.7668	1.3454	1.3454	90.0	45.7	91.4	-90.0	18.5	0.0	-12.4	-8.4
SeH_2---π(C_6H_6) (C_2: type II'_{Bzn})[f]	3.8660	1.4720	1.4720	90.0	45.4	90.7	90.0	-0.1	0.0	-12.5	-8.8
TeH_2---π(C_6H_6) (C_2: type II_{Bzn})	4.1343	1.6726	1.6726	90.0	45.4	90.8	90.0	-11.9	0.0	-11.6	-7.1
MP2 level (Counterpoise)											
HO-H---π(C_6H_6) (C_s: type Ia_{Bzn})	2.6282	0.9633	0.9606	77.5	155.2	104.2	-82.6	-149.2	0.0	-17.7[h]	-11.3[i]
HS-H---π(C_6H_6) (C_s: type Ib_{Bzn})	2.6311	1.3387	1.3373	85.0	137.4	92.9	-87.1	-149.9	180.0	-18.5[h]	-11.5[i]
HSe-H---π(C_6H_6) (C_s: type Ib_{Bzn})	2.6981	1.4586	1.4584	83.9	125.7	92.0	-86.4	-149.8	180.0	-20.0[h]	-12.5[i]
HTe-H---π(C_6H_6) (C_s: type Ib_{Bzn})	2.8190	1.6563	1.6583	83.2	114.3	91.3	-86.0	-149.7	180.0	-26.9[h]	-14.8[i]
OH_2---π(C_6H_6) (C_2: type II_{Bzn})	3.4452	0.9619	0.9619	90.0	51.7	103.3	90.0	-30.0	0.0	-16.8[h]	-11.1[i]
SH_2---π(C_6H_6) (C_2: type II_{Bzn})	3.8381	1.3381	1.3381	90.0	45.8	91.6	90.0	-30.0	0.0	-17.2[h]	-11.1[i]
SeH_2---π(C_6H_6) (C_2: type II_{Bzn})	3.9427	1.4584	1.4584	90.0	45.3	90.6	90.0	-30.0	0.0	-17.7[h]	-11.2[i]
TeH_2---π(C_6H_6) (C_2: type II_{Bzn})	4.1281	1.6563	1.6563	90.0	45.2	90.4	90.0	-30.0	0.0	-20.9[h]	-11.3[i]
SH_2---π(C_6H_6) (C_2: type II'_{Bzn})	3.8378	1.3381	1.3381	90.0	45.8	91.6	90.0	0.0	0.0	-17.2[h]	-11.1[i]
TeH_2---π(C_6H_6) (C_2: type II'_{Bzn})	4.1290	1.6563	1.6563	90.0	45.2	90.4	90.0	0.0	0.0	-20.9[h]	-11.3[i]

[a] See text for BSS-F. [b] $\Delta E_{ES} = E_{ES}((EH_2)\text{-}*\text{-}\pi(C_6H_6)) - (E_{ES}(EH_2) + E_{ES}(C_6H_6))$ on the energy surface. [c] $\Delta E_{ZP} = E_{ZP}((EH_2)\text{-}*\text{-}\pi(C_6H_6)) - (E_{ZP}(EH_2) + E_{ZP}(C_6H_6))$ with the zero-point energy corrections. [d] One imaginary frequency predicted for each. [e] Two imaginary frequencies predicted for each. [f] Each E–H points to C of C_6H_6 in type II'_{Bzn}. [g] Data from the weaker interaction. [h] ΔE_{raw}: Energies for the formation of the complexes uncorrected by the basis set superposition errors (E_{BSSE}). [i] ΔE_{BSSE}: Energies for the formation of the complexes corrected by E_{BSSE}.

contains the structural parameters optimized by applying the counterpoise correction method at the MP2 level and the energy for the formation of adducts, ΔE_{raw} (uncollected by E_{BSSE}) and ΔE_{BSSE} (collected by E_{BSSE}), for convenience of comparison.

Two types of structures were optimized for each adduct at the MP2 level. While HE–H---π(C_6H_6) (C_s: type Ia_{Bzn}) and EH_2---π(C_6H_6) (C_2: type II_{Bzn}) were optimized for E = O, HE–H---π(C_6H_6) (C_s: type Ib_{Bzn}) and EH_2---π(C_6H_6) (C_2: type II_{Bzn}) were for E = S, Se and Te. In the optimizations at the

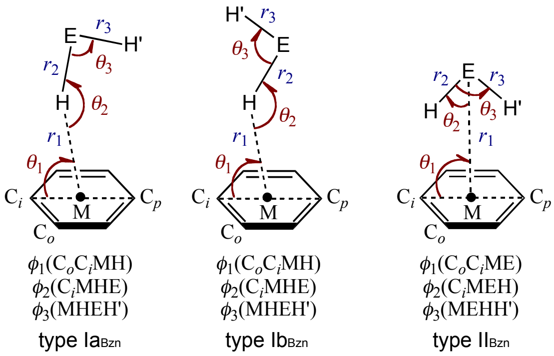

Scheme 1 Structural Parameters for (EH_2)---π(C_6H_6). The C_i atom in C_6H_6 is selected so as to the r(C_i---H) distance being shortest.

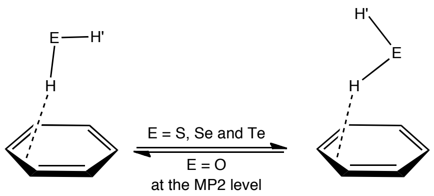

(4)

MP2 level, HE–H---π(C_6H_6) (C_s: type Ib_{Bzn}) converged to HE–H---π(C_6H_6) (C_s: type Ia_{Bzn}) for E = O, whereas HE–H---π(C_6H_6) (C_s: type Ia_{Bzn}) did to HE–H---π(C_6H_6) (C_s: type Ib_{Bzn}) for E = S, Se and Te (see eqn (4)). On the other hand, three types of structures were optimized for each of E = S, Se and Te in the EH_2 adduct with benzene π-system at the M06-2X and M06 levels, although only two types for E = O. The three types are HE–H---π(C_6H_6) (C_s/C_1: type Ia_{Bzn}), HE–H---π(C_6H_6) (C_s/C_1: type Ib_{Bzn}) and EH_2---π(C_6H_6) (C_2/C_1: type II_{Bzn}), where C_s/C_1 means C_s or C_1, for example. HO–H---π(C_6H_6) (C_s/C_1: type Ib_{Bzn}) was never optimized, although both HO–H---π(C_6H_6) (C_s/C_1: type Ia_{Bzn}) and EH_2---π(C_6H_6) (C_2/C_1: type II_{Bzn}) were at the M06 and M06-2X levels. Three types of structures (type Ia_{Bzn}, type Ib_{Bzn} and type II_{Bzn}) are illustrated in Chart 1.

Whereas HE–H---π(C_6H_6) (C_s: type Ia_{Bzn}/Ib_{Bzn}) (E = O, S, Se and Te) have all positive frequencies, one imaginary frequency was predicted for each of EH_2---π(C_6H_6) (C_2: type II_{Bzn}) at the MP2 level. The motion of the negative frequency does not connect the topologically duplicated HO–H---π(C_6H_6) (type Ia_{Bzn}), instead, it corresponds to the partial rotation of H_2O around the C_2 axis of the species, if evaluated with lower BSSs. The motion becomes to connect the topologically duplicated structures, if evaluated with higher BSSs. One imaginary frequency was similarly predicted for OH_2---π(C_6H_6) (C_1: type II_{Bzn}), even if the C_1 symmetry was assumed in the optimizations. OH_2---π(C_6H_6) (C_1: type II_{Bzn}) was very close to OH_2---π(C_6H_6) (C_2: type II_{Bzn}). Similar results were obtained for EH_2---π(C_6H_6) (C_1: type II_{Bzn}) (E = S, Se and Te) at the MP2 level. All positive frequencies were predicted for the optimized structures of the adducts at the M06 and M06-2X levels, except for HS–H---π(C_6H_6) (C_s: type Ib_{Bzn}) at the M06-2X level. Two lowest frequencies predicted for the species are collected in Table S1 of the Supporting Information. The results are well summarized in Table S1.

The intrinsic reaction coordinate method (IRC) was applied to those with one imaginary frequency, but it did not work. The energy surface around the minimum for the interaction must be very gradual in EH_2---π(C_6H_6) (E = O, S, Se and Te) at the MP2 level and HS–H---π(C_6H_6) (C_s: type Ib_{Bzn}) at the M06-2X level. The very gradual energy surface around the interactions would be responsible for the imaginary frequencies predicted for the species.[56]

Structures of SH_2---π(C_6H_6) (C_2) optimized at the M06-2X level and SeH_2---π(C_6H_6) (C_2) at the M06 level, which have all positive frequencies, are somewhat different from others. Each E–H bond points to C of C_6H_6 in the former two, whereas each E–H points to BCP of C=C in C_6H_6 for usual cases. The two structures are called SH_2---π(C_6H_6) (C_2: type II'_{Bzn}) and SeH_2---π(C_6H_6) (C_2: type II'_{Bzn}), respectively. While $\phi_2 \approx \pm 30°$ for the type II_{Bzn}, ϕ_2 are evaluated to be around 0° for type II'_{Bzn}, although not shown in Scheme 1. Similar structures are optimized for EH_2---π(C_6H_6) (C_2: type II'_{Bzn}) (E = S and Te) at the MP2 level. However, two imaginary frequencies are predicted for each. The motions correspond to the rotation around the C_2 axis and to the connection of the topologically duplicated HE–H---π(C_6H_6) (type Ia_{Bzn}). EH_2---π(C_6H_6) (C_2: type II'_{Bzn}) are slightly less stable than the corresponding type II_{Bzn}, for E = S and Te, evaluated at the MP2 level. EH_2---π(C_6H_6) (C_2: type II'_{Bzn}) converged to the type II_{Bzn} structures for E = O and Te. Table 1 also contains data for EH_2---π(C_6H_6) (C_2: type II'_{Bzn}).

How do the r_1 values in the adducts correlate between those evaluated at the MP2, M06-2X and M06 levels? Fig. 1 shows various plots for r_1: r_1 in EH_2---π(C_6H_6) (type II_{Bzn}) evaluated at the MP2 and M06 levels versus those evaluated at the M06-2X level for E = O, S, Se and Te; r_1 in HE–H---π(C_6H_6) (type Ia_{Bzn}) evaluated at M06 versus those at M06-2X for E = O, S, Se and Te and r_1 in HE–H---π(C_6H_6) (type Ib_{Bzn}) evaluated at M06 versus those at M06-2X for E = S, Se and Te. The plots gave excellent correlations, except for the correlation in the

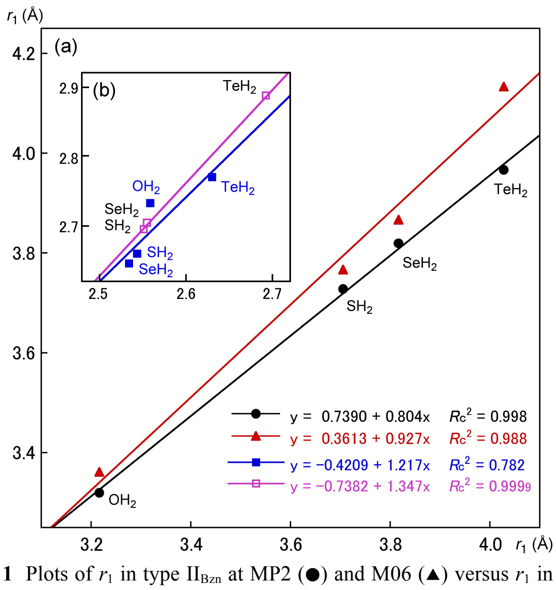

Fig. 1 Plots of r_1 in type II_{Bzn} at MP2 (●) and M06 (▲) versus r_1 in type II_{Bzn} at M06-2X ((a): figure outside) and the plot of r_1 in type Ia_{Bzn} at M06 versus r_1 in type Ia_{Bzn} at M06-2X (■) and the plot of r_1 in type Ib_{Bzn} at M06 versus r_1 in type Ib_{Bzn} at M06-2X (□) type ((b): figure inside).

plot of r_1 in HE–H---π(C_6H_6) (type Ia_{Bzn}) evaluated at M06 versus those at M06-2X for E = O, S, Se and Te. The correlations are given in the figure. Similar mechanisms are expected to operate in the determination of the r_1 values in II_{Bzn} and type Ib_{Bzn}, if the excellent correlations are detected as shown Fig. 1. How do the r_1 values correlate among the different types of structures? An excellent correlation is observed in the plot of r_1 in EH_2---π(C_6H_6) (C_2: type II_{Bzn}) versus r_1 in HE–H---π(C_6H_6) (C_s: type Ib_{Bzn}), evaluated at the MP2 level, for E = S, Se and Te, although it is not shown in the figure (y = 1.3726 + 1.023x; R_c^2 = 0.999_9). Similar mechanisms would also be emphasized to determine r_1 in type Ib_{Bzn} and type II_{Bzn}, if evaluated at the MP2 level.

The r_1 values elongated by 0.11–0.19 Å as shown in Table 1, if the counterpoise correction method is applied at the MP2 level, except for HO–H---π(C_6H_6) (C_s: type Ia_{Bzn}) of which elongation is 0.25 Å, although θ_1 and θ_2 affect much on r_1. The values are less than 0.03 Å at the M06-2X and M06 levels.

How are the stabilization energies in the formation of the adducts? The magnitudes of ΔE_{ES} are evaluated to be smaller in the order of MP2 > M06-2X > M06. The ΔE_{ES} values are predicted to be 17–21 kJ mol^{-1} with 27.3 kJ mol^{-1} for HTe–H---C_6H_6 (C_s: type Ib_{Bzn}) at the MP2 level, 13–18 kJ mol^{-1} at the M06-2X level and 11–15 kJ mol^{-1} at the M06 level. It seems difficult to find good correlations between ΔE for the adducts, although ΔE for EH_2---π(C_6H_6) (C_2/C_1: II_{Bzn}) seems inversely proportional to ΔE for HE–H---π(C_6H_6) (C_s/C_1; Ia_{Bzn}), if evaluated at the M06-2X for E = S, Se and Te (y = –20.9 – 0.451x: R_c^2 = 0.980).

The ΔE_{ZP} values are not so different from the ΔE_{ES} values, if evaluated at the MP2 level. The differences between the two ($\Delta E_{ZP:ES} = \Delta E_{ZP} - \Delta E_{ES}$) are –2 to 1 kJ mol^{-1}. The $\Delta E_{ZP:ES}$ values become larger and amount to 3–9 kJ mol^{-1} at the M06-2X and M06 levels. The ΔE_{raw} values seem close to the ΔE_{ES} values, if evaluated at the MP2 level. The contributions from E_{BSSE} destabilize the adducts substantially at the MP2 level (6–12 kJ mol^{-1}). While ΔE_{raw} are also close to ΔE_{ES} at the M06-2X and M06 levels, the contributions from E_{BSSE} become much smaller (see Table S3). The values are less than 2 kJ mol^{-1} at the M06-2X and M06 levels.

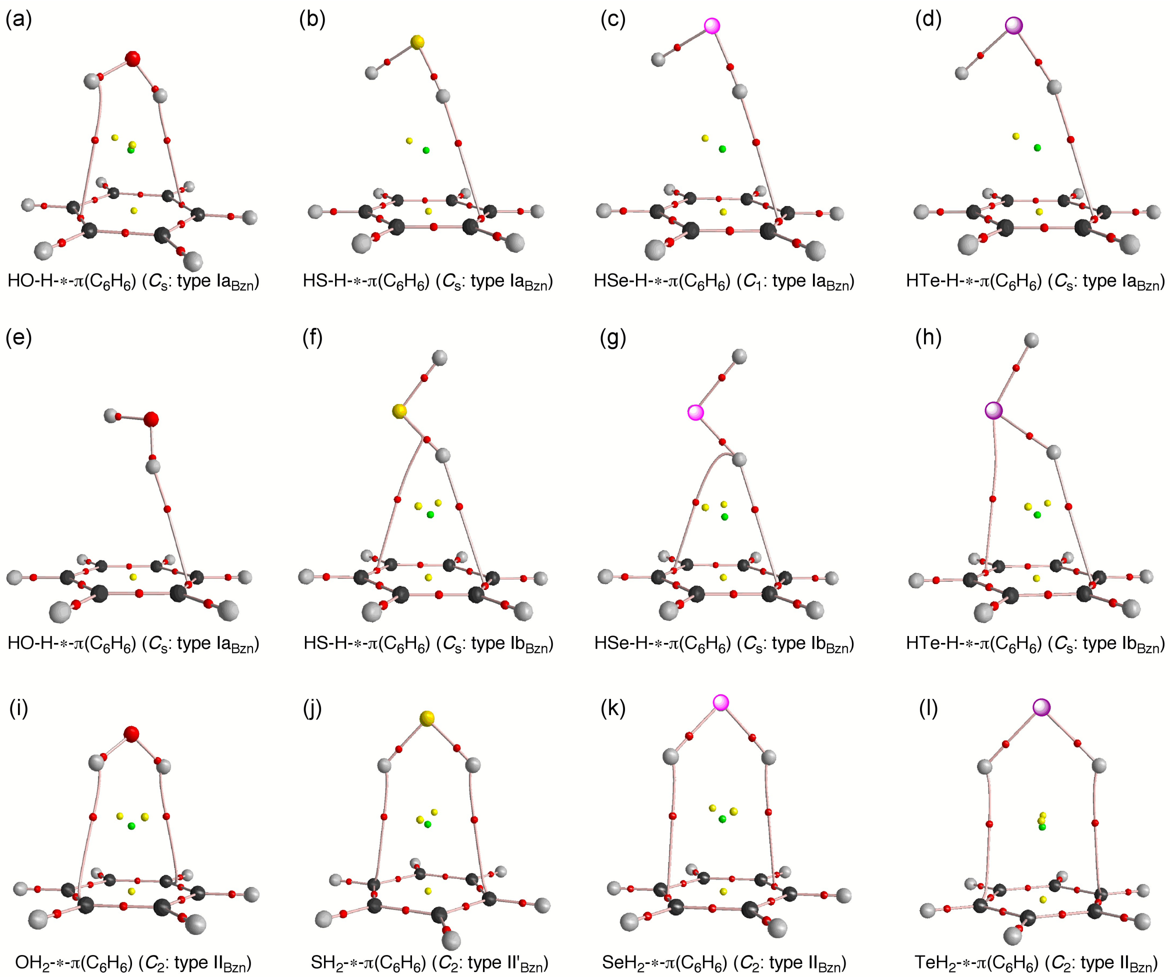

Fig. 2 Molcular graphs for HO–H-∗-π(C_6H_6) (C_s: type Ia_{Bzn}) (a), HS–H-∗-π(C_6H_6) (C_s: type Ia_{Bzn}) (b), HSe–H-∗-π(C_6H_6) (C_1: type Ia_{Bzn}) (c), HTe–H-∗-π(C_6H_6) (C_s: type Ia_{Bzn}) (d), HS–H-∗-π(C_6H_6) (C_s: type Ib_{Bzn}) (f), HSe–H-∗-π(C_6H_6) (C_s: type Ib_{Bzn}) (g), HTe–H-∗-π(C_6H_6) (C_s: type Ib_{Bzn}) (h), OH_2-∗-π(C_6H_6) (C_2: type II_{Bzn}) (i), SH_2-∗-π(C_6H_6) (C_1: type II'_{Bzn}) (j), SeH_2-∗-π(C_6H_6) (C_s: type II_{Bzn}) (k) and TeH_2-∗-π(C_6H_6) (C_2: type II_{Bzn}) (l), evaluated with M06-2X/BSS-F, together with HO–H-∗-π(C_6H_6) (C_s: type Ia_{Bzn}) (e), evaluated with MP2/BSS-F. The bond critical points (BCPs) are denoted by red dots (●), ring critical points (RCPs) by yellow dots (●) and cage critical points (CCPs) by green dots (●), together with bond paths by pink line (-●-). Carbon atoms are in black (●) and hydrogen atoms are in gray (●), with oxygen, sulfur, selenium and tellurium atoms in red (●), yellow (●), hot pink (●) and purple (●), respectively.

QTAIM-DFA is applied to the interactions in question. The purpose of this paper is to clarify the nature of the interactions in EH_2-∗-π(C_6H_6) (E = O, S, Se and Te). Therefore, interactions in the species with one imaginary frequency for each are similarly analyzed, for convenience of comparison. The species seems quasi-stable and never collapses to the component, even if it contains an imaginary frequency. The interaction, which is to be analyzed, is predicted to have the positive frequency, irrespective of the imaginary frequency for the lowest one.

Before detail discussion of the behavior of interactions by applying QTAIM-DFA, molecular graphs, contour plots, negative Laplacians and trajectory plots are examined, next.

Molecular graphs, contour plots, negative Laplacians and trajectory plots for (EH_2)-∗-π(C_6H_6) (E = O, S, Se and Te)

Fig. 2 illustrates the molecular graphs for HE–H-∗-π(C_6H_6) (C_s/C_1: type Ia_{Bzn}), HE–H-∗-π(C_6H_6) (C_s: type Ib_{Bzn}) and EH_2-∗-π(C_6H_6) (C_2/C_1: type II_{Bzn}) (E = O, S, Se and/or Te)

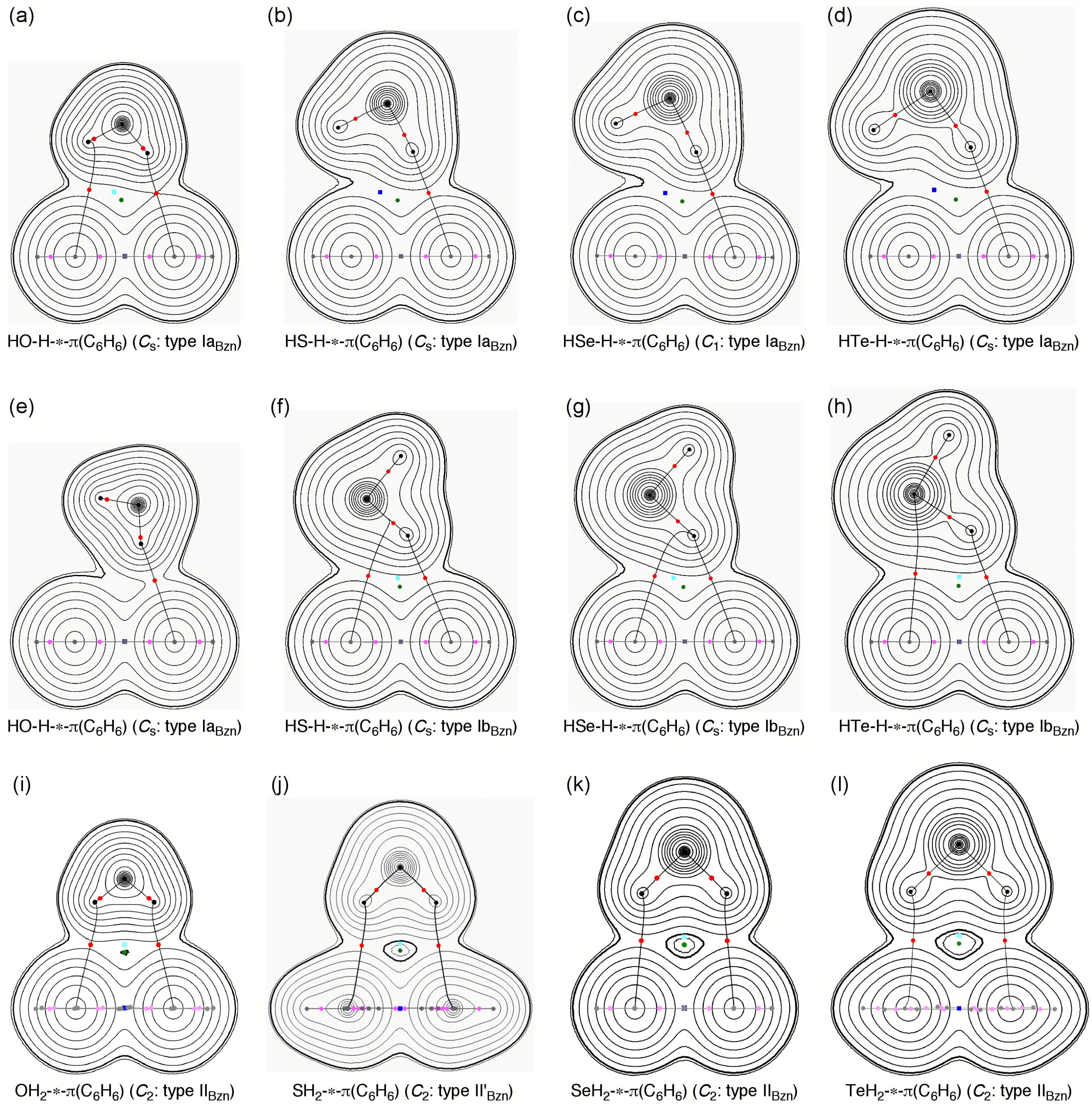

Fig. 3 Contour plots of $\rho_b(r_c)$ for HO–H-∗-π(C_6H_6) (C_s: type Ia_{Bzn}) (a), HS–H-∗-π(C_6H_6) (C_s: type Ia_{Bzn}) (b), HSe–H-∗-π(C_6H_6) (C_1: type Ia_{Bzn}) (c), HTe–H-∗-π(C_6H_6) (C_s: type Ia_{Bzn}) (d), HS–H-∗-π(C_6H_6) (C_s: type Ib_{Bzn}) (f), HSe–H-∗-π(C_6H_6) (C_s: type Ib_{Bzn}) (g), HTe–H-∗-π(C_6H_6) (C_s: type Ib_{Bzn}) (h), OH_2-∗-π(C_6H_6) (C_2: type II_{Bzn}) (i), SH_2-∗-π(C_6H_6) (C_1: type II'_{Bzn}) (j), SeH_2-∗-π(C_6H_6) (C_s: type II_{Bzn}) (k) and TeH_2-∗-π(C_6H_6) (C_2: type II_{Bzn}) (l), evaluated with M06-2X/BSS-F, together with HO–H-∗-π(C_6H_6) (C_s: type Ia_{Bzn}) (e), evaluated with MP2/BSS-F. Bond critical points (BCPs) on the plane are denoted by red dots (●), those outside of the plane in dark pink dots (●), ring critical points (RCPs) by blue squares (■), cage critical points (CCPs) by green dots (●) and bond paths on the plane by black line and those outside of the plane are by gray line. Carbon atoms are in black (●) and hydrogen atoms are in gray (●), with other atoms in black (●). The contours (ea_0^{-3}) are at 2^l (l = ±8, ±7, ..., 0) and 0.0047 (heavy line).

evaluated at the M06-2X level, together with OH_2-∗-π(C_6H_6) (C_2: type Ia_{Bzn}) evaluated at the MP2 level (see also Chart 1). All BCPs expected are clearly detected, containing those for the interactions in question, together with ring critical points (RCPs) and cage critical points (CCPs). The molecular graphs change depending on the calculation levels, employed for the evaluations, since the optimized structures somewhat change depending on the levels. Fig. 3 draws the contour plots of $\rho(\boldsymbol{r})$ on the C_s plane or that close to the plane for the species illustrated in Fig. 2. BCPs are well located at the three dimensional saddle points of $\rho(\boldsymbol{r})$ in the species. Figs. 4 and 5 draw the negative Laplacians and trajectory plots, respectively, for those in Fig. 2. It is well visualized how BCPs are classified through $\nabla^2\rho(\boldsymbol{r})$ and the space around the species is well divided into atoms in it, respectively.

Survey of Interactions in the EH_2 Adducts of Benzene π-System (E = O, S, Se and Te)

As shown in Figs. 2 and 3, some BPs curve apparently, as previously pointed out.[33] In such cases, the lengths of BPs (r_{BP}) will be substantially longer than the straight-line distances (R_{SL}). The r_{BP} values in question and those of the components (r_{BP-1} and r_{BP-2}: $r_{BP} = r_{BP-1} + r_{BP-2}$), evaluated at the MP2, M06-2X and M06 levels are summarized in Table

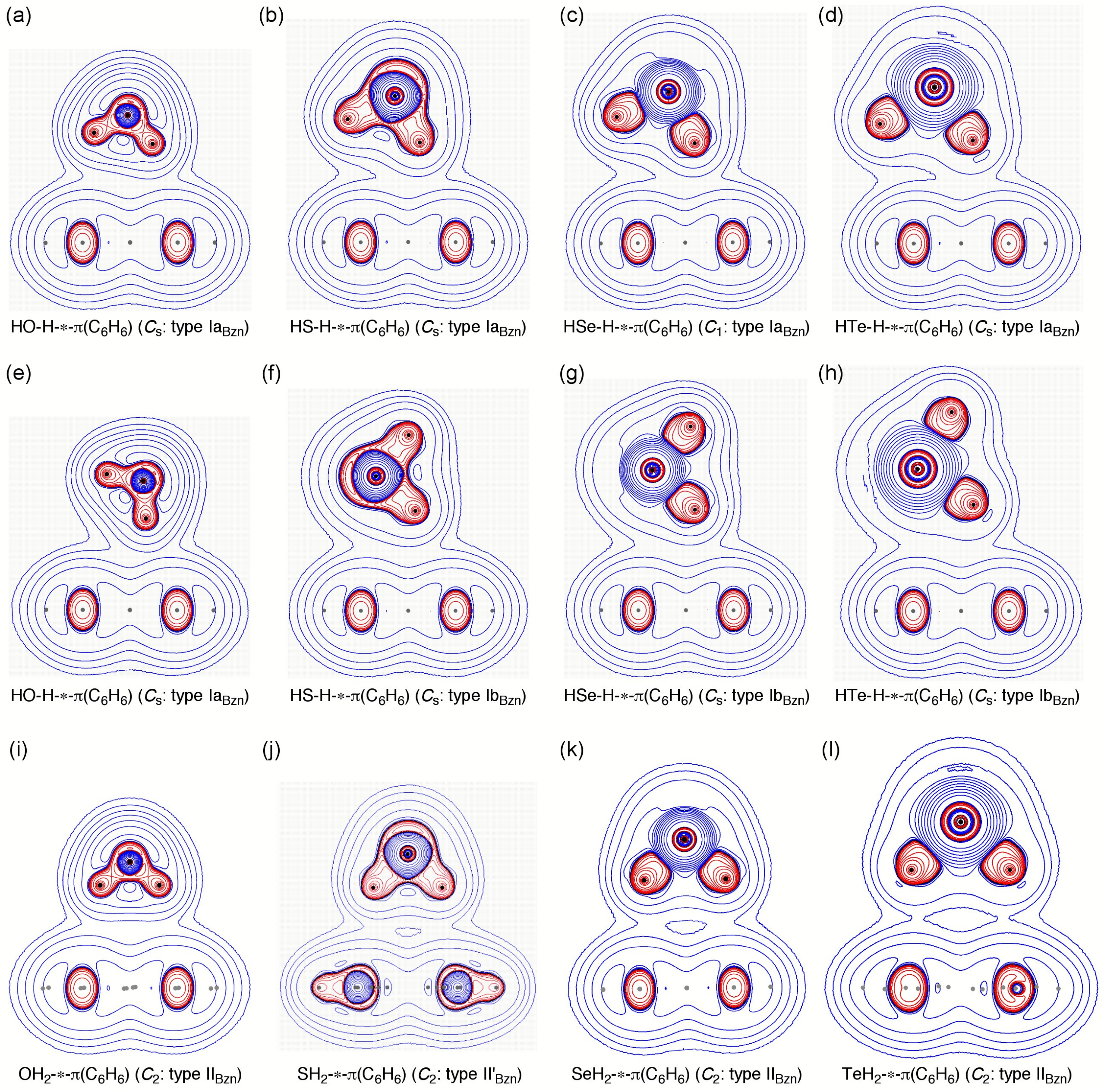

Fig. 4 Plots of Negative Laplacian for HO–H-∗-π(C_6H_6) (C_s: type Ia_{Bzn}) (a), HS–H-∗-π(C_6H_6) (C_s: type Ia_{Bzn}) (b), HSe–H-∗-π(C_6H_6) (C_1: type Ia_{Bzn}) (c), HTe–H-∗-π(C_6H_6) (C_s: type Ia_{Bzn}) (d), HS–H-∗-π(C_6H_6) (C_s: type Ib_{Bzn}) (f), HSe–H-∗-π(C_6H_6) (C_s: type Ib_{Bzn}) (g), HTe–H-∗-π(C_6H_6) (C_s: type Ib_{Bzn}) (h), OH_2-∗-π(C_6H_6) (C_2: type II_{Bzn}) (i), SH_2-∗-π(C_6H_6) (C_1: type II'_{Bzn}) (j), SeH_2-∗-π(C_6H_6) (C_2: type II_{Bzn}) (k) and TeH_2-∗-π(C_6H_6) (C_2: type II_{Bzn}) (l), evaluated with M06-2X/BSS-F, together with HO–H-∗-π(C_6H_6) (C_s: type Ia_{Bzn}) (e), evaluated with MP2/BSS-F. Positive and negative areas are shown by blue and red lines, respectively.

S4 of the Supporting Information. Fig. 6 shows the plot of r_{BP} *versus* R_{SL} for the interactions in question in the EH_2 adducts of benzene π-system (E = O, S, Se and Te), evaluated at the M06-2X level, for example. It is visualized that r_{BP} are very close to R_{SL} for most cases ($r_{BP} - R_{SL} < 0.03$ Å). An excellent correlation is obtained in the plot of r_{BP} versus R_{SL} for $r_{BP} - R_{SL} < 0.03$ Å, which is given in the figure. On the other hand, r_{BP} are larger than R_{SL} by 0.10–0.15 Å for the interactions in HO–H-∗-π(C_6H_6) (C_s: type Ia_{Bzn}), SH_2-∗-π(C_6H_6) (type II_{Bzn}: C_1) and TeH_2-∗-π(C_6H_6) (C_2: type II_{Bzn}). And further, r_{BP} are much larger than R_{SL} by 0.36–0.42 Å for those in HS–H-∗-π(C_6H_6) (C_s: type Ib_{Bzn}), HSe–H-∗-π(C_6H_6) (C_s: type Ib_{Bzn}) and OH_2-∗-π(C_6H_6) (C_2: type II_{Bzn}), as shown in Fig. 6.

Why the large differences between r_{BP} and R_{SL} are observed in these adducts? BPs in EH_2-∗-π(C_6H_6) (C_2: type II_{Bzn}) are expected to connect both H atoms in EH_2 and BCPs on the C=C bonds of C_6H_6 on the basis of their structural feature, at first glance. However, the H atoms are connected to the C atoms of C_6H_6 by BPs for E = O, S and Te. As a result, BPs

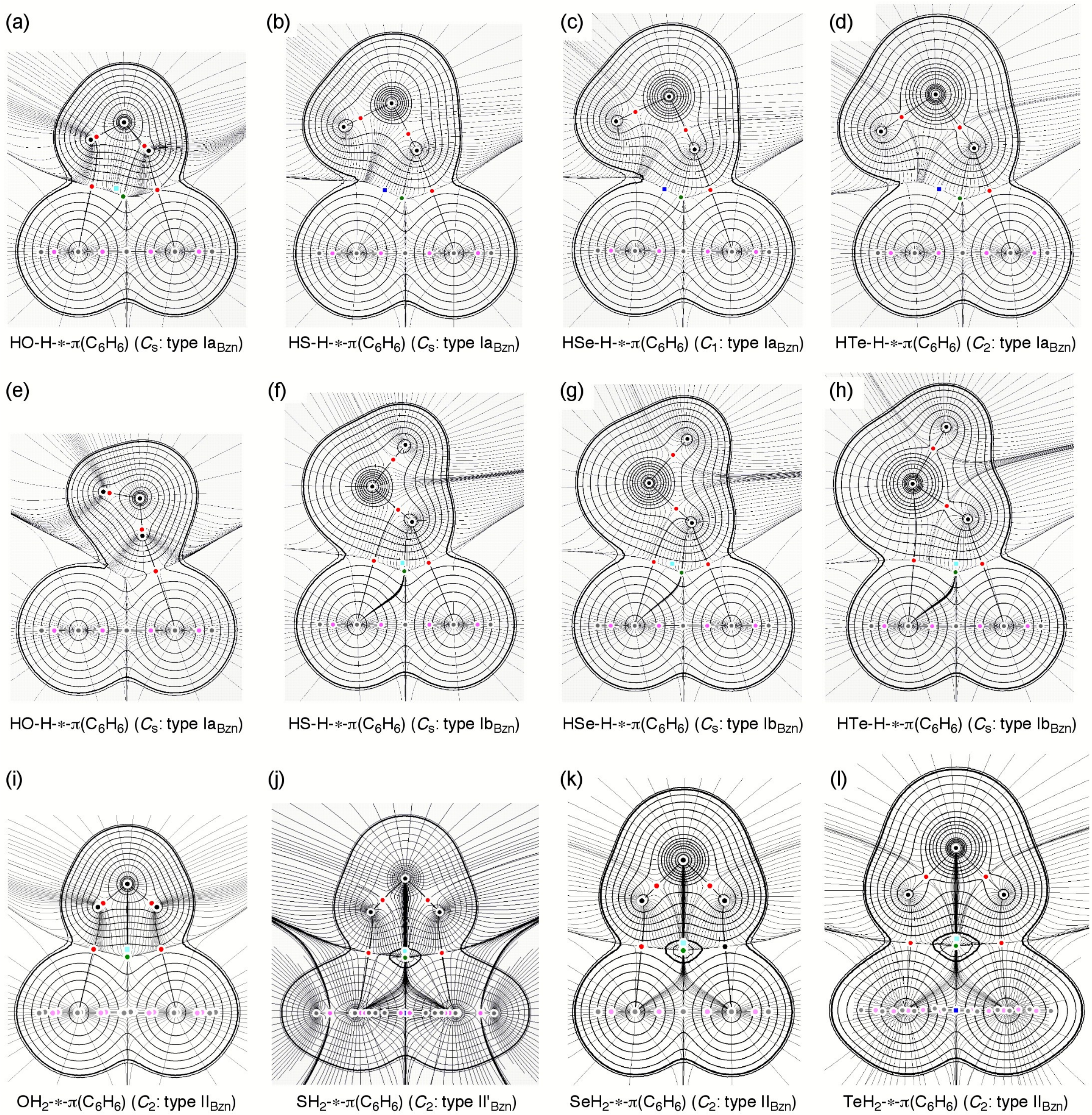

Fig. 5 Trajectory plots for HO–H-∗-π(C_6H_6) (C_s: type Ia_{Bzn}) (a), HS–H-∗-π(C_6H_6) (C_s: type Ia_{Bzn}) (b), HSe–H-∗-π(C_6H_6) (C_1: type Ia_{Bzn}) (c), HTe–H-∗-π(C_6H_6) (C_s: type Ia_{Bzn}) (d), HS–H-∗-π(C_6H_6) (C_s: type Ib_{Bzn}) (f), HSe–H-∗-π(C_6H_6) (C_s: type Ib_{Bzn}) (g), HTe–H-∗-π(C_6H_6) (C_s: type Ib_{Bzn}) (h), OH_2-∗-π(C_6H_6) (C_2: type II_{Bzn}) (i), SH_2-∗-π(C_6H_6) (C_1: type II'$_{Bzn}$) (j), SeH_2-∗-π(C_6H_6) (C_2: type II_{Bzn}) (k) and TeH_2-∗-π(C_6H_6) (C_2: type II_{Bzn}) (l), evaluated with M06-2X/BSS-F, together with HO–H-∗-π(C_6H_6) (C_s: type Ia_{Bzn}) (e), evaluated with MP2/BSS-F. Colors and marks are the same as those in Fig. 3.

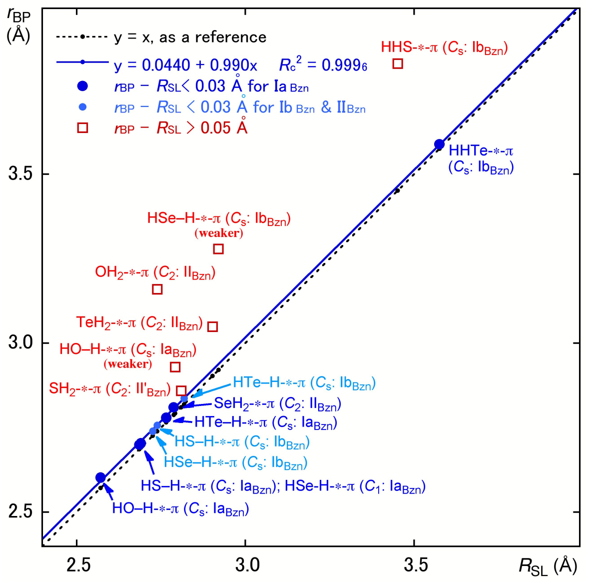

Fig. 6 Plot of r_{BP} versus R_{SL} for (EH_2)-∗-π(C_6H_6) (E = O, S, Se and Te), evaluated with BSS-F at the M06-2X level.

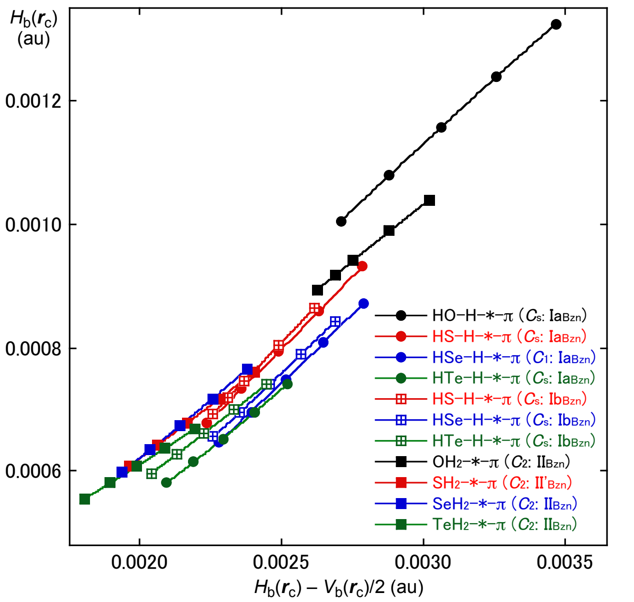

Fig. 7 Plots of $H_b(\mathbf{r}_c)$ versus $H_b(\mathbf{r}_c) - V_b(\mathbf{r}_c)/2$ for (EH_2)-∗-π(C_6H_6), evaluated with M06-2X/BSS-F. Colors and marks for the species are shown in the figure. Perturbed structures for OH_2-∗-π(C_6H_6) (C_s: II_{Bzn}) are generated employing w = –0.1, –0.05, 0, 0.025 and 0.05 in eqn (2), therefore, some intervals in the plot are shorter than others.

BPs will curve much around the C atoms, resulting in the large differences between r_{BP} and R_{SL} (see Figs. 2 and 3). In the case of SeH_2-∗-π(C_6H_6) (C_2: type II_{Bzn}), BPs connect BCPs on C=C of C_6H_6, as expected, therefore, $r_{BP} \approx R_{SL}$.

The R_{SL} values are expected to be larger in the order of E = O < S ≤ Se < Te, on the basis of the van der Waals radii of the atoms in the adducts. However, R_{SL} are predicted to be larger in the order of E = O < Se = Te < S for type II_{Bzn} at the MP2 level, for example. The results suggest the important contributions from the strengths of the interactions between EH_2 and benzene π-system in the adducts, which must be larger in the order of E = O < S < Se < Te. Namely, The combination of van der Waals radii of the atoms and strengths of the interactions will control the predicted order of R_{SL}, although the magnitudes of the contributions would change depending on the structures of the adducts and the calculation conditions.

Some BPs are observed to connect E in EH_2 and BCPs on C=C of C_6H_6 of HE–H-∗-π(C_6H_6) (C_s: type Ib_{Bzn}), in addition to the connection between H in HE–H and BCPs on C=C of C_6H_6. The interaction between E of EH_2 and BCPs on C=C of C_6H_6 in the adduct will be called the E-∗-π interaction. The structure HHE-∗-π(C_6H_6) (C_s: type Ib_{Bzn}) will be employed, instead of HE–H-∗-π(C_6H_6) (C_s: type Ib_{Bzn}), if it is necessary to emphasize the existence of the E-∗-π interaction. The E-∗-π interaction is clearly observed in HHE-∗-π(C_6H_6) (C_s: type Ib_{Bzn}) for E = Te and is narrowly detected for E = S, after careful examination, if evaluated at the M06-2X level (see Figs. 2 and 3). The appearance of E-∗-π changes depending on the evaluation levels. While the E-∗-π interaction is observed in HHE-∗-π(C_6H_6) (C_s: type Ib_{Bzn}) for E = Te at the MP2 level, they are detected for E = S and Te at the M06-2X level and for E = S, Se and Te at the M06 level.

QTAIM functions are calculated for the H-∗-π and E-∗-π interactions at BCPs in the species. Tables 2 and 3 collect the data, respectively. QTAIM-DFA is applied to the interactions in the species for E = O, S, Se and Te, evaluated at the MP2, M06-2X, and M06 levels. Fig. 7 show the plot of $H_b(\mathbf{r}_c)$ versus $H_b(\mathbf{r}_c) - V_b(\mathbf{r}_c)/2$ for the H-∗-π interactions in question, evaluated at the M06-2X level, for instance. All data in Fig. 7 appear in the area of $H_b(\mathbf{r}_c) - V_b(\mathbf{r}_c)/2 > 0$ and $H_b(\mathbf{r}_c) > 0$, which belong to the *pure* CS region, so do for E-∗-π, although not shown.

How is the behavior of the H-∗-π and E-∗-π interactions in question? QTAIM-DFA is applied to elucidate the behavior. The results will be discussed, next.

Application of QTAIM-DFA to H-∗-π in the EH_2 Adducts of Benzene π-system (E = O, S, Se and Te)

QTAIM-DFA parameters, (R, θ) and (θ_p, κ_p), are calculated for the H-∗-π and E-∗-π interactions in the EH_2 adducts of benzene π-system (E = O, S, Se and Te) at the MP2, M06-2X, and M06 levels, according to eqns (S3)–(S6) in the Supporting Information. The behavior of the H-∗-π and E-∗-π interactions will be discussed separately. Table 2 collects the QTAIM-DFA parameters, the frequencies correlated to NIV employed to generate the perturbed structures and the force constants, k_f, together with QTAIM functions, necessary to discuss the interactions in question.

The behavior of the H-∗-π interactions in the species are classified and characterized based on the QTAIM-DFA parameters of θ and θ_p, respectively, employing the typical values in Scheme S2, as a reference. It is instructive to survey the criteria briefly, closely related to those in this work. The interactions will be classified by the *pure* CS interactions if 45° < θ < 90° and the *regular* CS interactions for 90° < θ < 180°. On the other hand, the interactions will be characterized as the vdW nature for 45° ≤ θ_p < 90° and the typical HB nature without covalency for 90° < θ_p < 125°, where θ_p = 125° is the value tentatively determined corresponding to θ =

Table 2 QTAIM functions and QTAIM-DFA parameters for the (EH_2)-∗-π(C_6H_6) interactions, elucidated with QTAIM-DFA employing BSS-F at the MP2, M06-2X and M06 levels[a,b]

Species (X-∗-Y) (symmetry: type)	BCP at C_6H_6	$\rho_b(\boldsymbol{r}_c)$ (ea_o^{-3})	$c\nabla^2\rho_b(\boldsymbol{r}_c)^c$ (au)	$H_b(\boldsymbol{r}_c)$ (au)	$k_b(\boldsymbol{r}_c)^d$	R (au)	θ (°)	Freq. (cm^{-1})	k_f (unit)^e	θ_p (°)	κ_p (au^{-1})
MP2 level											
HO–H-∗-π(C_6H_6) (C_s: type Ia_{Bzn})	BCP	0.0085	0.0035	0.0014	-0.754	0.0038	68.5	102.0	0.034	66.6	39.0
HS–H-∗-π(C_6H_6) (C_s: type Ib_{Bzn})	BCP	0.0075	0.0028	0.0009	-0.815	0.0029	72.6	72.6	0.020	66.0	23.4
HSe–H-∗-π(C_6H_6) (C_s: type Ib_{Bzn})	BCP	0.0076	0.0027	0.0008	-0.824	0.0028	73.4	64.7	0.013	68.8	33.4
HTe–H-∗-π(C_6H_6) (C_s: type Ib_{Bzn})	BCP	0.0069	0.0024	0.0007	-0.826	0.0025	73.5	65.5	0.017	72.8	38.7
OH_2-∗-π(C_6H_6) (C_2: type II_{Bzn})	C	0.0059	0.0023	0.0007	-0.806	0.0024	72.0	95.4	0.032	71.3	33.9
SH_2-∗-π(C_6H_6) (C_2: type II_{Bzn})	C	0.0062	0.0021	0.0007	-0.814	0.0022	72.6	79.6	0.035	70.8	50.4
SeH_2-∗-π(C_6H_6) (C_2: type II_{Bzn})	C	0.0065	0.0021	0.0006	-0.820	0.0022	73.1	62.7	0.024	71.5	42.5
TeH_2-∗-π(C_6H_6) (C_2: type II_{Bzn})	C	0.0069	0.0022	0.0007	-0.820	0.0023	73.0	60.7	0.021	73.4	20.3
M06-2X level											
HO–H-∗-π(C_6H_6) (C_s: type Ia_{Bzn})	BCP	0.0078	0.0031	0.0012	-0.767	0.0033	69.3	125.5	0.049	67.1	30.9
	BCP^f	0.0063	0.0025	0.0008	-0.807	0.0026	72.1	125.5	0.049	73.8	93.6
HS–H-∗-π(C_6H_6) (C_s: type Ia_{Bzn})	BCP	0.0070	0.0025	0.0008	-0.811	0.0026	72.3	87.9	0.040	65.3	53.1
HSe–H-∗-π(C_6H_6) (C_1: type Ia_{Bzn})	BCP	0.0072	0.0025	0.0007	-0.825	0.0026	73.4	68.1	0.024	73.4	55.5
HTe–H-∗-π(C_6H_6) (C_s: type Ia_{Bzn})	BCP	0.0067	0.0023	0.0007	-0.834	0.0024	74.1	62.0	0.017	69.4	102.8
HS–H-∗-π(C_6H_6) (C_s: type Ib_{Bzn})	BCP	0.0064	0.0024	0.0007	-0.813	0.0025	72.5	79.3	0.030	64.5	6.6
HSe–H-∗-π(C_6H_6) (C_s: type Ib_{Bzn})	BCP	0.0069	0.0025	0.0007	-0.823	0.0026	73.2	73.8	0.014	66.5	52.8
	BCP^f	0.0064	0.0027	0.0011	-0.754	0.0029	68.4	280.6	0.048	76.2	408.1
HTe–H-∗-π(C_6H_6) (C_s: type Ib_{Bzn})	BCP	0.0064	0.0022	0.0007	-0.826	0.0023	73.5	64.6	0.020	70.5	66.7
OH_2-∗-π(C_6H_6) (C_2: type II_{Bzn})	C	0.0072	0.0028	0.0009	-0.794	0.0029	71.1	124.7	0.038	69.6	28.6
SH_2-∗-π(C_6H_6) (C_2: type II'_{Bzn})	C	0.0065	0.0022	0.0007	-0.814	0.0023	72.6	95.5	0.040	70.9	44.2
SeH_2-∗-π(C_6H_6) (C_2: type II_{Bzn})	BCP	0.0067	0.0021	0.0007	-0.813	0.0022	72.5	69.9	0.030	69.3	69.8
TeH_2-∗-π(C_6H_6) (C_2: type II_{Bzn})	C	0.0063	0.0020	0.0006	-0.820	0.0020	73.0	61.9	0.021	73.9	54.2
M06 level											
HO–H-∗-π(C_6H_6) (C_s: type Ia_{Bzn})	BCP	0.0072	0.0026	0.0009	-0.782	0.0028	70.3	111.6	0.041	67.8	9.1
	BCP^f	0.0041	0.0017	0.0006	-0.787	0.0018	70.6	53.7	0.008	75.9	132.1
HS–H-∗-π(C_6H_6) (C_s: type Ia_{Bzn})	BCP	0.0081	0.0026	0.0008	-0.805	0.0027	71.9	96.0	0.051	64.2	24.3
HSe–H-∗-π(C_6H_6) (C_s: type Ia_{Bzn})	BCP	0.0078	0.0025	0.0007	-0.831	0.0026	73.9	62.6	0.024	66.8	78.8
HTe–H-∗-π(C_6H_6) (C_s: type Ia_{Bzn})	BCP	0.0070	0.0022	0.0006	-0.846	0.0022	75.1	61.9	0.010	71.1	135.5
	BCP^f	0.0043	0.0014	0.0005	-0.772	0.0015	69.6	45.0	0.008	75.2	16.5
HS–H-∗-π(C_6H_6) (C_s: type Ib_{Bzn})	BCP	0.0056	0.0019	0.0006	-0.828	0.0020	73.6	57.9	0.008	70.3	145.9
HSe–H-∗-π(C_6H_6) (C_s: type Ib_{Bzn})	BCP	0.0058	0.0020	0.0006	-0.836	0.0021	74.2	63.7	0.021	69.0	88.2
HTe–H-∗-π(C_6H_6) (C_s: type Ib_{Bzn})	BCP	0.0048	0.0017	0.0005	-0.821	0.0017	73.1	70.6	0.011	78.3	24.5
OH_2-∗-π(C_6H_6) (C_2: type II_{Bzn})	C	0.0055	0.0020	0.0007	-0.798	0.0021	71.4	107.9	0.034	71.5	41.1
SH_2-∗-π(C_6H_6) (C_1: type II_{Bzn})	C	0.0060	0.0019	0.0006	-0.819	0.0020	73.0	95.9	0.050	70.5	89.3
SeH_2-∗-π(C_6H_6) (C_2: type II'_{Bzn})	C	0.0064	0.0019	0.0005	-0.840	0.0020	74.5	49.9	0.006	74.8	13.9
TeH_2-∗-π(C_6H_6) (C_2: type II_{Bzn})	C	0.0054	0.0017	0.0005	-0.832	0.0017	73.9	57.2	0.018	78.7	63.2

[a] See text for BSSs. [b] Data are given at BCP for interaction in question, which is shown by -∗-. [c] $H_b(\boldsymbol{r}_c) - V_b(\boldsymbol{r}_c)/2$, where $c = \hbar^2/8m$. [d] $k = V_b(\boldsymbol{r}_c)/G_b(\boldsymbol{r}_c)$. [e] mdyn $Å^{-1}$. [f] Data for the weaker interaction.

Table 3 QTAIM functions and QTAIM-DFA parameters for the E-∗-π interactions (π-EBs) in HHE-∗-π(C_6H_6) (C_s) of the Ib_{Bzn} type, evaluated with BSS-F at the MP2, M06-2X and M06 levels[a,b]

Species^c (X-∗-Y) (symmetry: type)	BCP at C_6H_6	$\rho_b(\boldsymbol{r}_c)$ (ea_o^{-3})	$c\nabla^2\rho_b(\boldsymbol{r}_c)^d$ (au)	$H_b(\boldsymbol{r}_c)$ (au)	$k_b(\boldsymbol{r}_c)^e$	R (au)	θ (°)	Freq. (cm^{-1})	k_f (unit)^f	θ_p (°)	κ_p (au^{-1})
MP2 level											
HHTe-∗-π(C_6H_6) (C_s: type Ib_{Bzn})	BCP	0.0083	0.0028	0.0009	-0.821	0.0030	73.1	71.3	0.013	78.3	80.6
M06-2X level											
HHS-∗-π(C_6H_6) (C_s: type Ib_{Bzn})	BCP	0.0065	0.0029	0.0011	-0.753	0.0031	68.4	66.9	0.010	69.3	1120
HHTe-∗-π(C_6H_6) (C_s: type Ib_{Bzn})	BCP	0.0071	0.0025	0.0008	-0.797	0.0026	71.3	85.6	0.016	74.5	82.6
M06 level											
HHS-∗-π(C_6H_6) (C_s: type Ib_{Bzn})	BCP	0.0049	0.0022	0.0009	-0.732	0.0024	67.1	83.2	0.035	72.6	2200
HHSe-∗-π(C_6H_6) (C_s: type Ib_{Bzn})	BCP	0.0053	0.0022	0.0009	-0.742	0.0024	67.7	73.4	0.012	72.5	850
HHTe-∗-π(C_6H_6) (C_s: type Ib_{Bzn})	BCP	0.0064	0.0021	0.0007	-0.788	0.0022	70.7	54.5	0.013	75.7	110

[a] See text for BSS-F. [b] Data are given at BCP for the interaction in question, which is shown by -∗-. [c] All frequencies are predicted to be positive for each species. [d] $H_b(\boldsymbol{r}_c) - V_b(\boldsymbol{r}_c)/2$, where $c = \hbar^2/8m$. [e] $k_b(\boldsymbol{r}_c) = V_b(\boldsymbol{r}_c)/G_b(\boldsymbol{r}_c)$. [f] mdyne $Å^{-1}$.

90º for the typical HB interactions without covalency.

The θ and θ_p values are less than 90º for all H-∗-π interactions in the EH_2 adducts of benzene π-system (E = O, S, Se and Te), evaluated in this work at the MP2, M06-2X, and M06 levels, as shown in Table 2. Consequently, it is concluded that all H-∗-π interactions in the species examined in this work are classified as the *pure* CS interactions and have the character of the vdW nature.

How are the behavior of the E-∗-π interactions in HHE-∗-π(C_6H_6)? The behavior is discussed, next.

Behavior of E-∗-π in the EH_2 Adducts of Benzene π-system, Elucidated with QTAIM-DFA

Table 3 collects the QTAIM-DFA parameters for the E-∗-π interactions in HHE-∗-π(C_6H_6) (C_s: type Ib_{Bzn}), together with the frequencies and the force constants (k_f), correlated to NIV employed to generate the perturbed structures. QTAIM functions are also contained in Table 3, necessary for the discussion of the interactions in question.

The θ and θ_p values in Table 3 are less than 90º for all E-∗-π interactions in HHE-∗-π(C_6H_6) (C_s: type Ib_{Bzn}). Consequently, it is also concluded that all E-∗-π interactions examined in this work are classified by the *pure* CS interactions and have the character of the vdW nature.

It is, however, worthwhile to comment that the θ_p value for the E-∗-π interaction seems larger than that of the H-∗-π interaction, if the θ_p values of the same species are compared, evaluated at the MP2 and M06-2X levels. The differences in θ_p [$\Delta\theta_p$ = θ_p(E-∗-π) − θ_p(H-∗-π)] amount to 4.0º–5.5º, if evaluated at the MP2 and M06-2X levels. The results show that E-∗-π has the nature of the stronger interactions than the case of H-∗-π for the dynamic behavior in the same species. However, we must be careful when the $\Delta\theta_p$ values are discussed in relation to the strength of the interactions, since the $\Delta\theta_p$ value could be negative, if evaluated at the M06 level. The $\Delta\theta_p$ value is evaluated to be –2.6º for HHTe-∗-π(C_6H_6) (C_s: type Ib_{Bzn}), if evaluated at the M06 level. The Te-∗-π interaction in HHTe-∗-π(C_6H_6) (C_s: type Ib_{Bzn}) and/or the H-∗-π interaction in HTe–H-∗-π(C_6H_6) (C_s: type Ib_{Bzn}) would not be suitably evaluated at the M06 level. The results strongly suggest that the E-∗-π interaction has the nature of the stronger interactions than the case of H-∗-π for the dynamic behavior in the same EH_2 adduct of benzene π–system (E = S, Se and Te) under our calculation conditions.

Investigations on the behavior of similar interactions in naphthalene π-system are in progress.

Conclusion

The behavior of the H-∗-π interactions is elucidated by applying QTAIM-DFA for the EH_2 adducts of benzene π–system (E = O, S, Se and Te), together with the E-∗-π interactions detected in the same species. Structures were optimized with BSS-F at the MP2, M06-2X and M06 levels. Three types of structures (type Ia_{Bzn}, type Ib_{Bzn} and type II_{Bzn}) were optimized for the adducts (Chart 1). All positive frequencies were predicted for the optimized structures, except for EH_2---π(C_6H_6) (C_2: type II_{Bzn}) (E = O, S, Se and Te) at MP2 and HS–H---π(C_6H_6) (C_s: type Ib_{Bzn}) at M06-2X. The very gradual energy surface around the interaction in the species would be responsible for the imaginary frequency. Some BPs curve apparently in the molecular graphs and the contour plots dawn on the optimized structures. In these cases, the lengths of BPs (r_{BP}) are substantially longer than the straight-line distances (R_{SL}).

QTAIM-DFA is applied to the H-∗-π and E-∗-π interactions in the EH_2 adducts of benzene π–system (E = O, S, Se and Te). QTAIM-DFA parameters are calculated (Tables 2 and 3). The θ and θ_p values are less than 90º for all H-∗-π and E-∗-π interactions in the species, examined in this work. Consequently, all H-∗-π and E-∗-π interactions (E = O, S, Se and Te) are classified as the *pure* CS interactions and characterized to have the vdW-*nature*. However, the θ_p values for the E-∗-π interactions are evaluated to be larger than those of the H-∗-π interactions by 4.0º–5.5º (= θ_p(π-EB) – θ_p(π-HB) = $\Delta\theta_p$) if θ_p in the same species are compared, evaluated at the MP2 and M06-2X levels. The results strongly suggest that the E-∗-π interaction has the nature of the stronger interactions than the case of H-∗-π for the dynamic behavior in the same EH_2 adduct of benzene π–system (E = S, Se and Te).

Acknowledgements

This work was partially supported by a Grant-in-Aid for Scientific Research (Nos. 23350019 and 26410050) from the Ministry of Education, Culture, Sports, Science and Technology, Japan. The support of the Wakayama University Original Research Support Project Grant and the Wakayama University Graduate School Project Research Grant is also acknowledged.

Notes and references

[a] *Department of Material Science and Chemistry, Faculty of Systems Engineering, Wakayama University, 930 Sakaedani, Wakayama 640-8510, Japan. Fax: +81 73 457 8253; Tel: +81 73 457 8252; E-mail: hayashi3@sys.wakayama-u.ac.jp*

† Electronic supplementary information (ESI) available: Cartesian coordinates for optimized structures of (EH_2)---π(C_6H_6) (E = O, S, Se and Te). For ESI or other electronic format see DOI: 10.1039/b000000x.

1 L. Pauling, *The Nature of the Chemical Bond*, ed. L. Pauling, Cornell University Press, Ithaca, NY, 1960, 3rd ed.
2 G. C. Pimentel and A. L. McClellan, *The Hydrogen Bond*; W. H. Freeman: San Francisco, CA, 1960.
3 *The Hydrogen Bond, Recent Developments in Theory and Experiments*, eds. P. Schuster, G. Zundel and C. Sandorfy, North-Holland Publishing Company, Amsterdam, 1976.
4 G. A. Jeffrey and W. Saenger, *Hydrogen Bonding in Biological Structures*, Springer, Berlin, 1991.
5 G. A. Jeffrey, *An Introduction to Hydrogen Bonding*; Oxford University Press: New York, 1997.
6 A. D. Buckingham, A. C. Legon and S. M. Roberts, *Principles of Molecular Recognition*; Blackie Academic & Professional: London, 1993.
7 S. Scheiner, *Hydrogen Bonding, A Theoretical Perspective*, Oxford University Press, Oxford, 1997.
8 G. R. Desiraju and T. Steiner, *The Weak Hydrogen Bond in Structural Chemistry and Biology; International Union of Crystallography Monographs on Crystallography*: Oxford University Press, New York, 1999.
9 *Hydrogen Bonding – New Insights, Vol. 3, Challenges and Advances in Computational Chemistry and Physics*; ed. S. J. Grabowski, Springer, The Netherlands, Dordrecht, 2006.
10 G. Buemi, *Intramolecular Hydrogen Bonds. Methodologies and Strategies for Their Strength Evaluation.* In *Hydrogen Bonding – New Insights*, *Vol. 3, Challenges and Advances in Computational Chemistry and Physics*; ed. S. J. Grabowski, Springer, The Netherlands, Dordrecht, 2006, ch. 2, pp. 51–107.
11 K.-L. Han and G.-J. Zhao, *Hydrogen Bonding and Transfer in the Excited State*; John Wiley & Sons Ltd, UK, 2010.

12 (*a*) M. Nishio, *The CH/π Interaction: Evidence, Nature, and Consequences*, Wiley-VCH, New York, 1998; (*b*) M. Nishio, *Cryst. Eng. Comm.*, 2004, **6**, 130−158; (*c*) O. Takahashi, Y. Kohno and M. Nishio, *Chem. Rev.*, 2010, **110**, 6049–6076.

13 (*a*) E. Espinosa, E. Molins and C. Lecomte. *Chem. Phys. Lett.*, 1998, **285**, 170–173; (*b*) E. Espinosa, M. Souhassou, H. Lachekar and C. Lecomte, *Acta Crystallogr. B*, 1999, **55**, 563–572; (*c*) E. Espinosa, C. Lecomte and E. Molins, *Chem. Phys. Lett.*, 1999, **300**, 745–748; (*d*) E. Espinosa, I. Alkorta, I. Rozas, J. Elguero and E. Molins, *Chem. Phys. Lett.*, 2001, **336**, 457–461; (*e*) C. Gatti and L. Bertini, *Acta Crystallogr A*, 2004, **60**, 438–449.

14 (*a*) R. Parthasarathi, V. Subramanian and N. Sathyamurthy, *J. Phys. Chem. A*, 2006, **110**, 3349–3351; (*b*) R. Parthasarathi, V. Subramanian and N. Sathyamurthy, *J. Phys. Chem. A*, 2007, **111**, 13287–13290.

15 (*a*) S. J. Grabowski, *Chem. Phys. Lett.*, 1999, **312**, 542–547; (*b*) S. J. Grabowski, *Chem. Phys. Lett.*, 2000, **327**, 203–208; (*c*) A. J. Rybarezk, S. J. Grabowski and J. Nawrot-Modranka, *J. Phys. Chem. A*, 2003, **107**, 9232–9239; (*d*) S. J. Grabowski, *J. Phys. Org. Chem.*, 2004, **17**, 18–31; (*e*) S. J. Grabowski, T. L. Robinson and J. Leszczynski, *Chem. Phys. Lett.*, 2004, **386**, 44–48; (*f*) S. J. Grabowski, *Ann. Rep. Prog. Chem., Sect. C*, 2006, **102**, 131–165; (*g*) S. J. Grabowski, *Croat. Chem. Acta*, 2009, **82**, 185–192; (*h*) F. Fuster and S. J. Grabowski, *J. Phys. Chem. A*, 2011, **115**, 10078–10086.

16 (*a*) T. Steiner and W. Saenger, *J. Am. Chem. Soc.*, 1993, **115**, 4540–4547; (*b*) T. Steiner, *Angew. Chem., Int. Ed.*, 2002, **41**, 48–76.

17 W. H. Latimer and W. H. Rodebush, *J. Am. Chem. Soc.*, 1920, **42**, 1419–1433.

18 (*a)* P. L. A. Popelier and R. F. W. Bader, *Chem. Phys. Lett.*, 1992, **189**, 542–548; (*b*) D. K. Taylor, I. Bytheway, D. H. R. Barton and M. B. Hall, *J. Org. Chem.*, 1995, **60**, 435–444.

19 U. Koch and P. L. A. Popelier, *J. Phys. Chem.*, 1995, **99**, 9747–9754.

20 T. W. Martin and Z. S. Derewenda, *Nat. Struct. Biol.*, 1999, **6**, 403–406.

21 G. Gilli and P. Gilli, *J. Mol. Struct.*, 2000, **552**, 1–15.

22 P. Hobza and Z. Havlas, *Chem. Rev.*, 2000, **100**, 4253–4264.

23 G. R. Desiraju, *Acc. Chem. Res.*, 2002, **35**, 565–573.

24 K. N. Robertson, O. Knop and T. S. Cameron, *Can. J. Chem.*, 2003, **81**, 727–743.

25 O. Knop, K. N. Rankin and R. J. Boyd, *J. Phys. Chem. A*, 2003, **107**, 272–284.

26 A. Volkov and P. Coppens, *J. Comput. Chem,* 2004, **25**, 921–934.

27 H. K. Woo, X. B. Wang, L. S. Wang and K. C. Lu, *J. Phys. Chem. A*, 2005, **109**, 10633–10637.

28 J. E. Del Bene and J. Elguero, *J. Phys. Chem. A*, 2005, **109**, 10759–10769.

29 J. Thar and B. Kirchner, *J. Phys. Chem. A*, 2006, **110**, 4229–4237.

30 A. Mohajeri and F. F. Nobandegani, *J. Phys. Chem. A*, 2008, **112**, 281–295.

31 H. Szatyłowicz, *J. Phys. Org. Chem.*, 2008, **21**, 897–914.

32 M. Zgarbov, P. Jurecka, P. Banas, M. Otyepka, J. E. Sponer, N. B. Leontis, C. L. Zirbel and J. Sponer, *J. Phys. Chem. A*, 2011, **115**, 11277–11292.

33 Y. Sugibayashi, S. Hayashia and W. Nakanishi, *Phys Chem. Chem. Phys.,* 2015, **17**, 28879–28891.

34 The adducts between EH_2 and $\pi(C_6H_6)$ will be called type I_{Bzn}, if the components in (EH_2)-∗-$\pi(C_6H_6)$ are connected by only one BP for each, whereas they will be type II_{Bzn}, when they are joined through two BPs for each. However, it is difficult to determine the types before drawing the molecular graphs, therefore, the types are often given tentatively based on the structural similarities.

35 (*a*) *Atoms in Molecules. A Quantum Theory*, ed. R. F. W. Bader, Oxford University Press, Oxford, UK, 1990; (*b*) C. F. Matta and R. J. Boyd, *An Introduction to the Quantum Theory of Atoms in Molecules* In *The Quantum Theory of Atoms in Molecules: From Solid State to DNA and Drug Design*, ed. C. F. Matta and R. J. Boyd, Wiley-VCH, Weinheim, Germany, 2007, ch. 1.

36 A chemical bond or an interaction between A and B is denoted by A–B, which corresponds to bond paths (BP) between A and B in QTAIM. A-∗-B is employed here to emphasize the presence of BCP on A–B.

37 (*a*) S. Suzuki, P. G. Green, R. E. Bumgarner, S. Dasgupta, W. A. Goddard III and G. A. Blake, *Science*, 1992, **257**, 942–945; see also (*b*) R. N. Pribble and T. S. Zwier, *Science*, 1994, **265**, 75–79; (*c*) X. Wang and P. P. Power, *Angew. Chem. Int. Ed.*, 2011, **50**, 10965–10968.

38 K. P. Gierszal, J. G. Davis, M. D. Hands, D. S. Wilcox, L. V. Slipchenko and D. Ben-Amotz, *J. Phys. Chem. Lett.*, 2011, **2**, 2930–2933.

39 J. Ma, D. Alfè, A. Michaelides and E. Wang, *J. Chem. Phys.*, 2009, **130**, 154303-1–154303-6.

40 L. Bondesson, E. Rudberg, Y. Luo and P. Słek, *J. Comput. Chem.*, 2008 29, 1725–1732.

41 S. Li, V. R. Cooper, T. Thonhauser, A. Puzder and D. C. Langreth, *J. Phys. Chem. A*, 2008, **112**, 9031–9036.

42 (*a*) R. F. W. Bader, T. S. Slee. D. Cremer and E. Kraka, *J. Am. Chem. Soc.*, 1983, **105**, 5061–5068; (*b*) R. F. W. Bader, *Chem. Res.*, 1991, **91**, 893–928; (*c*) R. F. W. Bader, *J. Phys. Chem. A*, 1998, **102**, 7314–7323; (*d*) F. Biegler-König, R. F. W. Bader and T. H. Tang, *J. Comput. Chem.*, 1982, **3**, 317–328; (*e*) R. F. W. Bader, *Acc. Chem. Res.*, 1985, **18**, 9–15; (*f*) T. H. Tang, R. F. W. Bader and P. MacDougall, *Inorg. Chem.*, 1985, **24**, 2047–2053; (*g*) F. Biegler-König, J. Schönbohm and D. Bayles, *J. Comput. Chem.*, 2001, **22**, 545–559; (*h*) F. Biegler-König and J. Schönbohm, *J. Comput. Chem.*, 2002, **23**, 1489–1494.

43 J. Molina and J. A. Dobado, *Theor. Chem. Acc.*, 2001, **105**, 328–337.

44 J. A. Dobado, H. Martinez-Garcia, J. Molina and M. R. Sundberg, *J. Am. Chem. Soc.*, 2000, **122**, 1144–1149.

45 (*a*) W. Nakanishi, S. Hayashi and K. Narahara, *J. Phys. Chem. A*, 2009, **113**, 10050–10057; (*b*) W. Nakanishi, S. Hayashi and K. Narahara, *J. Phys. Chem. A*, 2008, **112**, 13593–13599.

46 W. Nakanishi and S. Hayashi, *Curr. Org. Chem.*, 2010, **14**, 181–197.

47 W. Nakanishi and S. Hayashi, *J. Phys. Chem. A*, 2010, **114**, 7423–7430.

48 W. Nakanishi, S. Hayashi, K. Matsuiwa and M. Kitamoto, *Bull. Chem. Soc. Jpn.*, 2012, **85**, 1293–1305.

49 *Gaussian 09 (Revision D.01)*, M. J. Frisch, G. W. Trucks, H. B. Schlegel, G. E. Scuseria, M. A. Robb, J. R. Cheeseman, G. Scalmani, V. Barone, B. Mennucci, G. A. Petersson, H. Nakatsuji, M. Caricato, X. Li, H. P. Hratchian, A. F. Izmaylov, J. Bloino, G. Zheng, J. L. Sonnenberg, M. Hada, M. Ehara, K. Toyota, R. Fukuda, J. Hasegawa, M. Ishida, T. Nakajima, Y. Honda, O. Kitao, H. Nakai, T. Vreven, J. A. Montgomery, Jr., J. E. Peralta, F. Ogliaro, M. Bearpark, J. J. Heyd, E. Brothers, K. N. Kudin, V. N. Staroverov, R. Kobayashi, J. Normand, K. Raghavachari, A. Rendell, J. C. Burant, S. S. Iyengar, J. Tomasi, M. Cossi, N. Rega, J. M. Millam, M. Klene, J. E. Knox, J. B. Cross, V. Bakken, C. Adamo, J. Jaramillo, R. Gomperts, R. E. Stratmann, O. Yazyev, A. J. Austin, R. Cammi, C. Pomelli, J. W. Ochterski, R. L. Martin, K. Morokuma, V. G. Zakrzewski, G. A. Voth, P. Salvador, J. J. Dannenberg, S. Dapprich, A. D. Daniels, Ö. Farkas, J. B. Foresman, J. V. Ortiz, J. Cioslowski and D. J. Fox, Gaussian, Inc.: Wallingford CT, 2009.

50 For the 6-311G(3d) basis sets, see: (*a*) R. C. Binning Jr. and L. A. Curtiss, *J. Comput. Chem.*, 1990, **11**, 1206–1216; (*b*) L. A. Curtiss, M. P. McGrath, J.-P. Blaudeau, N. E. Davis, R. C. Binning Jr. and L. Radom, *J. Chem. Phys.*, 1995, **103**, 6104–6113; (*c*) M. P. McGrath and L. Radom, *J. Chem. Phys.*, 1991, **94**, 511–516. For the diffuse functions (+ and ++), see: T. Clark, J. Chandrasekhar, G. W. Spitznagel and P. v. R. Schleyer, *J. Comput. Chem.*, 1983, **4**, 294–301.

51 From Sapporo Basis Set Factory: T. Noro, M. Sekiya and T. Koga, *Theoret. Chem. Acc.*, 2012, **131**, 1124.

52 (*a*) C. Møller and M. S. Plesset, *Phys. Rev.*, 1934, **46**, 618–622; J. Gauss, *J. Chem. Phys.*, 1993, **99**, 3629–3643; (*b*) J. Gauss, *Ber. Bunsen-Ges. Phys. Chem.*, 1995, **99**, 1001–1008.

53 Y. Zhao and D. G. Truhlar, *Theor. Chem. Acc.* 2008, **120**, 215–241.

54 The AIM2000 program (Version 2.0) is employed to analyze and visualize atoms-in-molecules: F. Biegler-König, *J. Comput. Chem.*, 2000, **21**, 1040−1048. See also ref 42g.

55 S. Hayashi, K. Matsuiwa, M. Kitamoto and W. Nakanishi, *J. Phys. Chem. A*, 2013, **117**, 1804–1816.

56 The results are not improved, even if the optimizations are performed under the Opt = VTight and SCF = Tight conditions, assuming both C_2 and C_1 symmetries for the adducts.

Graphical contents entry.

The nature of the π-HB and π-EB interactions are elucidated for (EH_2)-∗-π(C_6H_6) (E = O, S, Se and Te) by applying QTAIM-DFA. All interactions were classified by the *pure* CS interactions and characterized as the vdW-*nature*, with the suggestion of stronger π-EBs, relative to π-HBs, for the dynamic behavior, in the same adduct.

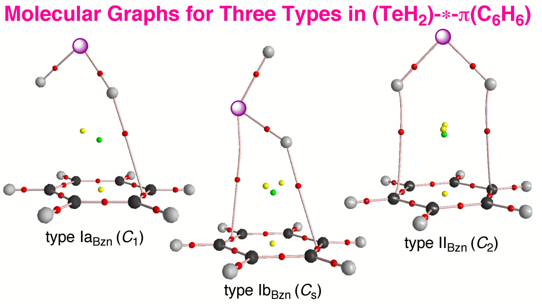

Keywords: ab initio calculations / atoms-in-molecules (AIM) / benzene π adduct / hydrogen bonds / structure / through-bond interactions